ORNL/SUB/99-19XSY063V-2

ORNL
Master Copy

MAR 16 1999

ornl

OAK RIDGE
NATIONAL
LABORATORY

LOCKHEED MARTIN

Evaluation of Mixed LEU-MOX Loading Patterns for LWRs Originating from Inability to Deliver MOX Assemblies

(Westinghouse Reload Core Study)

Imelda Ariani
Paul J. Turinsky

MANAGED AND OPERATED BY
LOCKHEED MARTIN ENERGY RESEARCH CORPORATION
FOR THE UNITED STATES
DEPARTMENT OF ENERGY

ORNL-27 (3-96)

SUB00146

This report was prepared as an account of work sponsored by an agency of the United States Government. Neither the United States Government nor any agency thereof, nor any of their employees, makes any warranty, express or implied, or assumes any legal liability or responsibility for the accuracy, completeness, or usefulness of any information, apparatus, product, or process disclosed, or represents that its use would not infringe privately owned rights. Reference herein to any specific commercial product, process, or service by trade name, trademark, manufacturer, or otherwise, does not necessarily constitute or imply its endorsement, recommendation, or favoring by the United States Government or any agency thereof. The views and opinions of authors expressed herein do not necessarily state or reflect those of the United States Government or any agency thereof.

ORNL/SUB/99-19XSY063V-2

EVALUATION OF MIXED LEU-MOX LOADING PATTERNS FOR LWRs ORIGINATING FROM INABILITY TO DELIVER MOX ASSEMBLIES

(Westinghouse Reload Core Study)

Imelda Ariani
Paul J. Turinsky

Date Published: February 1999

Report Prepared by
LOCKHEED MARTIN ENERGY RESEARCH CORP.
P.O. Box 2008
Oak Ridge, Tennessee 37831-6363
under
Subcontract Number 85B99398V

Funded by
Office of Fissile Materials Disposition
United States Department of Energy

Prepared for

Computational Physics and Engineering Division
Oak Ridge National Laboratory
Oak Ridge, Tennessee 37831
managed by
LOCKHEED MARTIN ENERGY RESEARCH CORP.
for the
U.S. DEPARTMENT OF ENERGY
under contract DE-96OR22464

FINAL REPORT

Evaluation of Mixed LEU-MOX Loading Patterns for LWRs Originating from Inability to Deliver MOX Assemblies

Westinghouse Reload Core Study

Imelda Ariani and Paul J. Turinsky

Electric Power Research Center
Department of Nuclear Engineering
North Carolina State University
Raleigh, NC

January, 1999

Contents

1. Introduction 1
2. Methodology 2
3. Lattice Physics Predictions 3
4. Equilibrium Cycle, Full MOX Core 3
5. Initial Mixed LEU-MOX Core 15
6. Subsequent Mixed LEU-MOX Cores 19
   - 6.1 Scenario 1: MOX Feed Batches Available for Subsequent Cycle 20
   - 6.2 Scenario 2: MOX Feed Batches Continue to be Unavailable for Subsequent Cycle 23
   - 6.3 Transition Back to Full LEU Core 25
   - 6.4 Summary of Key Core Attributes 27
7. Conclusions 30
8. Acknowledgment 30
9. References 30

List of Figures

FIGURE 1. Equilibrium Cycle, Full MOX Core Loading Pattern 7

FIGURE 2. PHOENIX/ANC vs. HELIOS/FORMOSA-P Assembly Burnup at 0.15 GWd/MTM 8

FIGURE 3. PHOENIX/ANC vs. HELIOS/FORMOSA-P Assembly Power at 0.15 GWd/MTM 8

FIGURE 4. PHOENIX/ANC vs. HELIOS/FORMOSA-P Peak Pin Power at 0.15 GWd/MTM 9

FIGURE 5. PHOENIX/ANC vs. HELIOS/FORMOSA-P Assembly Burnup at 11 GWd/MTM 9

FIGURE 6. PHOENIX/ANCvs.HELIOS/FORMOSA-PAssemblyPowerat11GWd/MTM 10

FIGURE 7. PHOENIX/ANCvs.HELIOS/FORMOSA-PPeakPinPowerat11GWd/MTM 10

FIGURE 8. PHOENIX/ANC vs. HELIOS/FORMOSA-P Assembly Burnup at 21.564 GWd/MTM 11

FIGURE 9. PHOENIX/ANC vs. HELIOS/FORMOSA-P Assembly Power at 21.564 GWd/MTM 11

FIGURE 10. PHOENIX/ANC vs. HELIOS/FORMOSA-P Peak Pin Power at 21.564 GWd/MTM 12

FIGURE 11. PHOENIX/ANC versus HELIOS/FORMOSA-P Peak FDH 12

FIGURE 12. PHOENIX/ANC versus HELIOS/FORMOSA-P Boron Coefficients 13

FIGURE 13. PHOENIX/ANC versus HELIOS/FORMOSA-P MTC 13

FIGURE 14. Equilibrium Cycle, Full MOX Core Key Attributes at BOC Conditions ..14

FIGURE 15. Equilibrium Cycle, Full MOX Core Key Attributes at EOC Conditions..14

FIGURE 16. Mixed Core Scenarios 17

FIGURE 17. Initial Mixed Core Loading Pattern 18

FIGURE 18. Initial Mixed Core Key Attributes at BOC Conditions 18

FIGURE 19. Initial Mixed Core Key Attibutes at EOC Conditions 19

FIGURE 20. Scenario 1 Loading Pattern 21

FIGURE 21. Scenario 1 Core Key Attributes at BOC Conditions 21

FIGURE 22. Pin Power Distribution in Scenario 1 22

List of Figures

FIGURE 23. Scenario 1 Core Key Attributes at EOC Conditions 22
FIGURE 24. Scenario 2 Loading Pattern 23
FIGURE 25. Scenario 2 Core Key Attributes at BOC Conditions 24
FIGURE 26. Scenario 2 Core Key Attributes at EOC Conditions 24
FIGURE 27. Full LEU Core Loading Pattern 25
FIGURE 28. Full LEU Core Key Attributes at BOC Conditions 26
FIGURE 29. Full LEU Core Key Attributes at EOC Conditions 26
FIGURE 30. Soluble Boron Concentration vs. Cycle Burnup 28
FIGURE 31. Peak FDH vs. Cycle Burnup 28
FIGURE 32. HFP Boron Worth vs. Cycle Burnup 29
FIGURE 33. HFP MTC vs. Cycle Burnup 29

List of Tables

TABLE 1: Core Design and Operating Parameters 7

TABLE 2: Feed Enrichment for Various Cores 27

TABLE 3: Core Performance for Various Cores 27

1. Introduction

This study is in support of the weapon's grade Pu disposition project utilizing the reactor option, which entails burning weapon's grade Mixed Oxide (MOX) fuel in Light Water Reactors (LWRs). What is being evaluated is the feasibility of substituting Low Enriched Uranium (LEU) fuel assemblies for weapon's grade MOX assemblies starting from an equilibrium cycle, full MOX core. The specific focus of this report is on the Westinghouse Pressurized Water Reactor (PWR) core design, starting with an equilibrium cycle, full MOX core identified by Westinghouse [1]. The motivation for this study is two fold. Firstly, since there are technical and political uncertainties associated with the utilization of weapon's grade MOX assemblies, there is a potential that some or all of the feed fuel assemblies associated with a reload region may not be available in a timely manner. This condition will be referred to as the disruption scenario. Secondly, at the conclusion of the Pu disposition campaign, the reactors involved will need to transition back to full LEU cores. Either condition will result in the insertion of feed LEU assemblies in a core containing once and twice burnt weapon's grade MOX assemblies. There are known design challenges associated with mixed LEU-MOX cores. Work to date has addressed transitioning from an equilibrium cycle, full LEU core to an equilibrium cycle, full MOX core. The emphasis of the current study is noted to be related to the reverse transition, with the additional complexity of not knowing when this will occur for the disruption scenario.

The design features of interest include the lattice design and core loading pattern (LP). The lattice design involves the placement of fuel and burnable poison (BP) material within the fuel lattice. The lattice designs used in this study for both MOX and LEU lattices have been restricted to existing Westinghouse designs, with lattice average enrichment and BP loading as free decision variables. In determining the LP, most active LP constraints have been imposed, the exception being the shutdown margin constraint.

2. Methodology

To complete the mixed LEU-MOX core assessment, core simulator models must be established. This involves generating two-group, homogenized cross-sections via a lattice physics code and solving the two-group neutron diffusion equation via a core simulator code. The lattice physics code that was employed in this study is the HELIOS code [2]. HELIOS employs the Current Coupling Collision Probability (CCCP) method to solve the integral form of the neutron transport equation. The many-group cross-section library is based upon ENDF/B-VI. The resonance treatment employs the subgroup method. The core simulator that was employed is the FORMOSA-P code [3]. FORMOSA-P solves the two-dimensional (radial), two-group neutron diffusion equation utilizing the Nodal Expansion Method (NEM) based upon quartic polynomials. The microscopic depletion option of FORMOSA-P has been utilized to better represent interfacial effects at LEU-MOX assembly interfaces. Pin-power reconstruction is completed utilizing intra-nodal fluxes and pin-power form factors, correcting for spatially dependent, spectral history effects. Pin burnups are evaluated based solely upon the intra-nodal burnup distribution. The unique feature of FORMOSA-P is the incorporation of a mathematical optimization capability to determine the near-optimum LPs for a stated objective function within imposed constraints. This is done utilizing the simulated annealing, stochastic optimization method and adaptive penalty functions. In determining the LP, the feed enrichment and BP loadings of the feed assemblies are also determined to satisfy cycle energy requirement and maximum soluble boron limit, respectively. The objective utilized throughout most of this study is the minimization of the feed enrichment of the dominant feed batch, this objective function being a surrogate for minimizing the feed region cost.

To link HELIOS to FORMOSA-P, the ZENITH [2] and FORCIP-P [4] codes were employed. ZENITH can read and process the output files of HELIOS as directed by user input provided in a higher level language, *e.g.* mathematical formulas. FORCIP-P was modified to read the ZENITH output file, manipulate the cross-sections to the form required by FORMOSA-P, and create the FORMOSA-P cross-section input file.

3. Lattice Physics Predictions

Lattice physics calculations for fuel and non-fuel lattices were completed by the team from Texas A&M University utilizing HELIOS/ZENITH codes. HELIOS lattice physics calculations were completed for a range of MOX and LEU lattice designs, spanning different fuel enrichments and BP loadings. This provided the lattice design inventory from which FORMOSA-P selected, with fuel enrichment treated as a continuous decision variable and BP loading as an integer decision variable. For MOX assemblies, Wet Annular Burnable Absorber (WABA) rods were employed; whereas, for LEU assemblies Integral Fuel Burnable Absorber (IFBA) were employed. This was done to avoid using integral burnable absorber in MOX pins, a restriction placed on the design by DOE due to lack of burnup experience for such a configuration. For each lattice design, the lattice was depleted to high burnup at base case conditions, *i.e.* Hot Full Power (HFP) average moderator density and fuel temperature. Multiple instantaneous branch cases were executed during the depletion, enabling characterization of the cross-sections as a function of moderator density, fuel temperature and soluble boron concentration within FORMOSA-P in order to apply spatially dependent, feedback corrections.

4. Equilibrium Cycle, Full MOX Core

Table 1 provides the core design and operating parameters assumed throughout this study. A FORMOSA-P model has been established for the equilibrium cycle, full MOX core identified by Westinghouse [1]. This model not only provided the starting basis to evaluate subsequent reload cores, but allowed FORMOSA-P predictions of core attributes to be contrasted with those of the Westinghouse core simulator ANC for this core. Note that the cross-sections used by ANC are generated using the PHOENIX lattice physics code. An equilibrium cycle, full MOX core is established in FORMOSA-P in an iterative manner. Beginning-of-Cycle (BOC) assembly quadrant isotopics, associated with the 2x2 spatial radial mesh/assembly being employed, are initially estimated by assuming them uniform across the assembly, obtaining the isotopics from HELIOS utilizing the ANC predicted assembly average burnups. This initialization process ignores both the assembly quadrant-wise spatial dependence and core position dependent spectral history effects. In addition, equilibrium *Sm* conditions are initially assumed at BOC, in error since feed assemblies have no *Sm* and burned assemblies have peak *Sm*. These initialization

approximations are necessary based upon the information available. The cycle is then depleted utilizing FORMOSA-P, and BOC reestablished based upon the End-of-Cycle (EOC) isotopics and appropriate *Sm* conditions predicted by FORMOSA-P. This process is repeated until BOC attributes converge. For each cycle, the ANC predicted critical soluble boron values are employed, and FORMOSA-P completes a critical axial buckling search. This is necessary, since FORMOSA-P is a two-dimensional code. The implication is that contrasting ANC and FORMOSA-P predicted critical soluble boron values is meaningless. Also note that the equilibrium cycle, full MOX core identified by Westinghouse utilizes 40 w/o ^{10}B isotopic abundance in the soluble boron to keep critical boron concentrations at manageable levels. Hence, all cores derived from this equilibrium cycle, full MOX core utilize 40 w/o ^{10}B in the soluble boron.

The equilibrium cycle, full MOX core loading pattern is shown in Figure 1. Key core attributes as predicted by FORMOSA-P at BOC and EOC conditions are shown in Figure 14 and Figure 15, respectively. For BOC, equilibrium Xenon and peak Samarium (burnt assemblies)/ no Samarium (fresh assemblies) fission product conditions are used. All constraints are noted to be satisfied for this core, as predicted by the FORMOSA-P model.

BOC, MOC, and EOC comparisons between HELIOS/FORMOSA-P and PHOENIX/ ANC of predicted core attributes are presented in Figure 2 through Figure 9. At BOC, since PHOENIX/ANC results for 0 GWd/MTM are not available, comparisons are instead presented at 0.15 GWd/MTM. Poorer agreements (compared to HELIOS/FORMOSA-P versus DIT/ROCS for the ABB-CE core) are noted. For the HELIOS/FORMOSA-P versus DIT/ROCS comparisons, we also completed a comparison between HELIOS versus DIT lattice predictions, to both assure that the HELIOS model setup was correct and predicted values are consistent. For the full MOX Westinghouse core, lattice results from PHOENIX were not available, so a comparison between HELIOS versus PHOENIX lattice predictions could not be completed. In addition, we are now contrasting a macroscopic depletion based core simulator, ANC, with a microscopic depletion based core simulator, FORMOSA-P, which may provide a reason for some of the differences observed.

Figure 2 indicates that at BOC, the burnt assemblies all have lower burnups as predicted by HELIOS/FORMOSA-P versus PHEONIX/ANC. Since an equilibrium cycle is being analyzed, further insight into the cause of the differences in BOC burnt assembly burnups can be obtained from Figure 8, which presents the EOC assembly burnup distribution. There it can be seen that the burnups of the highest burnt assemblies, *i.e.* those to be discharge, are higher and the remaining burnt assemblies, *i.e.* those to be reloaded, are lower as predicted by HELIOS/FORMOSA-P, which is to be expected since total core average assembly burnup must be preserved. Given these differences in EOC assembly burnups, one would expect that the highest and remaining burnt assemblies' powers should be lower and higher, respectively, as predicted by HELIOS/FORMOSA-P versus PHEONIX/ANC. Figure 9 indicates that this is not the case, indicating that the likely cause of the differences noted are due to HELIOS versus PHOENIX differences, *e.g.* lattice k_{inf} versus burnup curve differences, and not due to FORMOSA-P and ANC differences.

Figure 3, which presents the BOC assembly power distribution, indicates that the HELIOS/FORMOSA-P model shows an out-in radial assembly power distribution tilt versus PHOENIX/ANC. Based upon a sensitivity study completed, it is not obvious that the BOC assembly burnup distribution differences presented in Figure 2 are the source of this power distribution tilt. By EOC, the power distribution tilt has reversed to an in-out tilt due to HELIOS/FORMOSA-P under-burning the core periphery with reference to PHOENIX/ANC, which can be seen in Figure 8. Peak pin power differences at BOC, MOC and EOC are shown in Figure 4, Figure 7 and Figure 10, respectively. Figure 11 presents the radial peaking factor, $F_{\Delta H}$, versus cycle burnup. It can be seen that HELIOS/FORMOSA-P generally predicts lower peak pin powers than PHOENIX/ANC for the lead fuel assemblies, with differences as large as 0.05 in relative power. Much of this difference can be attributed to the difference in predicted nodal power. Again, without access to the PHOENIX results, one can only conjecture that HELIOS versus PHOENIX differences are the major source for the peak pin power prediction differences.

Figure 12 contrasts the HFP boron reactivity worths as a function of cycle burnup as predicted by HELIOS/FORMOSA-P and PHOENIX/ANC. Generally good agreement is obtained until higher cycle burnups, where now predicted boron worths differ by up to 3 pcm/ppm. The HFP moderator temperature coefficient (MTC) predicted values versus

cycle burnup are contrasted in Figure 13, where excellent agreement over the total cycle is noted.

The FORMOSA-P equilibrium cycle, full MOX core model just critiqued, provides the starting point for the mixed LEU-MOX core study.

TABLE 1: Core Design and Operating Parameters

Parameter	Value
Number of Fuel Assemblies	193
Fuel Lattice	17x17
Fuel Rods / Assembly	264
Active Fuel Height (in.)	144
Power Level (MWth)	3565
HFP Core Average Linear Power Density (kW/ft.)	5.68
HFP Core Power Density (kW/l)	109.21
HFP Moderator Inlet Temperature (^{o}F)	556.6
HFP Core Average Temperature Rise (^{o}F)	59.6
Core Loading (MTM)	81.6
Number of Feed Assemblies	92
Target Cycle Length (MWd/MTM)	21,564
Pin Discharge Burnup Limit (MWd/MTM)	60,000
Assembly Discharge Burnup Limit (MWd/MTM)	57,000
Region Discharge Burnup Limit (MWd/MTM)	45,000
Peak $F_{\Delta H}$ Limit	1.528

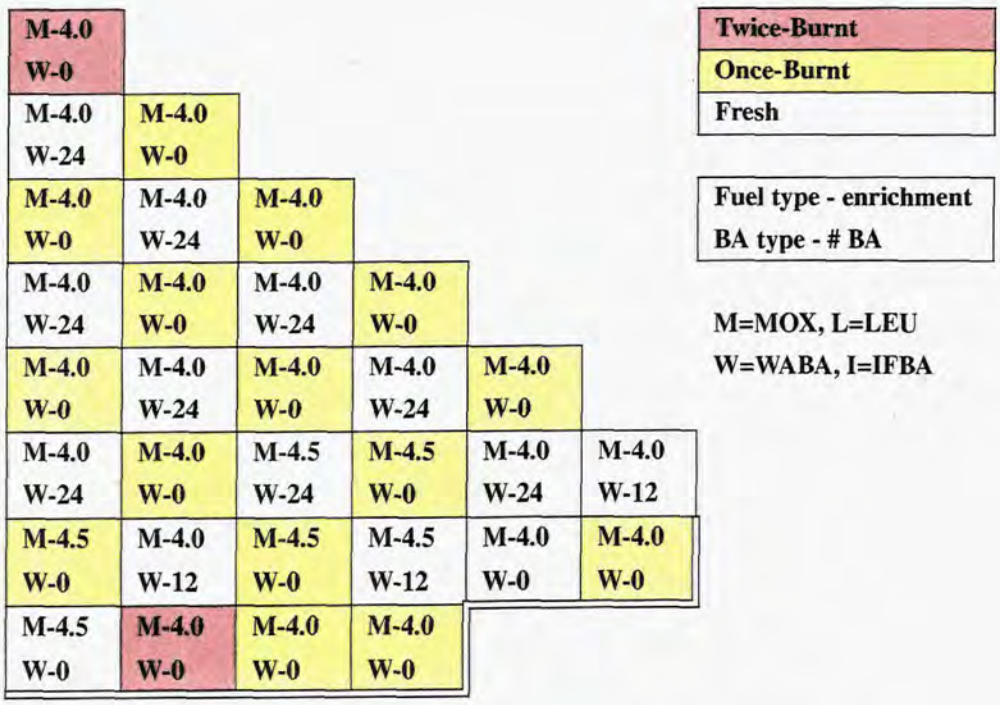

FIGURE 1. *Equilibrium Cycle, Full MOX Core Loading Pattern*

35.664			PHOENIX/ANC		
35.322			HELIOS/FORMOSA-P		
0.342			Difference		
0.175	24.743		Twice-Burnt MOX		
0.176	24.500		Once-Burnt MOX		
-0.001	0.243		Fresh MOX		
26.687	0.180	26.527			
26.321	0.181	26.231	unit = GWD/MTM		
0.366	-0.001	0.296			
0.181	27.005	0.185	24.753		
0.181	26.692	0.186	24.511		
0.000	0.313	0.001	0.242		
26.922	0.184	26.899	0.191	20.832	
26.603	0.183	26.585	0.192	20.665	
0.319	0.001	0.314	-0.001	0.167	
0.184	23.670	0.188	22.285	0.179	0.151
0.182	23.428	0.186	22.049	0.182	0.155
0.002	0.242	0.002	0.236	-0.005	-0.004
16.524	0.166	26.889	0.160	0.140	27.004
16.184	0.163	26.543	0.160	0.142	26.708
0.340	0.003	0.346	0.000	-0.002	0.296
0.113	29.902	18.726	27.066		
0.107	29.457	18.512	26.775		
0.006	0.445	0.214	0.291		

FIGURE 2. PHOENIX/ANC vs. HELIOS/FORMOSA-P Assembly Burnup at 0.15 GWd/MTM

0.921			PHOENIX/ANC		
0.934			HELIOS/FORMOSA-P		
-.013			Difference		
1.171	1.062				
1.176	1.089				
-.005	-.027				
1.051	1.202	1.069			
1.078	1.209	1.098			
-.027	-.007	-.029			
1.205	1.061	1.228	1.122		
1.209	1.087	1.233	1.146		
-.004	-.026	-.005	-.024		
1.069	1.222	1.088	1.266	1.162	
1.087	1.219	1.108	1.266	1.176	
-.018	0.007	-.020	0.000	-.014	
1.227	1.087	1.246	1.169	1.181	0.997
1.214	1.090	1.234	1.176	1.190	1.011
0.013	-.003	0.012	-.007	-.009	-.014
1.101	1.114	0.907	1.062	0.931	0.427
1.072	1.096	0.906	1.054	0.926	0.422
0.029	0.018	0.001	0.008	0.005	0.005
0.766	0.485	0.471	0.363		
0.728	0.458	0.444	0.348		
0.038	0.027	0.027	0.015		

FIGURE 3. PHOENIX/ANC vs. HELIOS/FORMOSA-P Assembly Power at 0.15 GWd/MTM

0.972 0.976 -0.004					
1.308 1.297 0.011	1.141 1.154 -0.013				
1.128 1.143 -0.016	1.332 1.325 0.008	1.154 1.171 -0.017			
1.332 1.323 0.009	1.143 1.155 -0.012	1.372 1.361 0.011	1.232 1.239 -0.007		
1.150 1.154 -0.004	1.349 1.333 0.016	1.178 1.185 -0.007	1.397 1.390 0.007	1.268 1.280 -0.012	
1.347 1.333 0.014	1.177 1.184 -0.007	1.424 1.400 0.024	1.257 1.264 -0.007	1.372 1.353 0.020	1.288 1.292 -0.004
1.294 1.279 0.015	1.311 1.299 0.012	1.078 1.073 0.005	1.314 1.317 -0.003	1.297 1.322 -0.025	0.767 0.784 -0.017
1.065 1.040 0.025	0.750 0.692 0.058	0.783 0.730 0.053	0.601 0.600 0.001		

PHOENIX/ANC
HELIOS/FORMOSA-P
Difference

FIGURE 4. PHOENIX/ANC vs. HELIOS/FORMOSA-P Peak Pin Power at 0.15 GWd/MTM

46.075 46.013 0.062					
13.251 13.251 0.000	36.541 36.662 -0.121				
38.343 38.347 -0.004	13.482 13.503 -0.021	38.285 38.380 -0.095			
13.464 13.462 0.002	38.675 38.725 -0.050	13.609 13.606 0.003	36.861 36.959 -0.098		
38.605 38.604 0.001	13.527 13.477 0.050	38.685 38.694 -0.009	13.769 13.703 0.066	33.121 33.111 0.010	
13.454 13.337 0.117	35.425 35.358 0.067	13.635 13.493 0.142	34.673 34.556 0.117	12.581 12.467 0.114	10.582 10.461 0.121
28.326 27.875 0.451	12.119 11.935 0.184	36.852 36.564 0.288	11.400 11.205 0.195	9.735 9.488 0.247	31.681 31.269 0.412
8.430 8.078 0.352	35.441 34.790 0.651	24.193 23.754 0.439	31.232 30.800 0.432		

PHOENIX/ANC
HELIOS/FORMOSA-P
Difference

Unit = GWd/MTM

FIGURE 5. PHOENIX/ANC vs. HELIOS/FORMOSA-P Assembly Burnup at 11 GWd/MTM

0.989 1.008 -0.019					
1.244 1.224 0.020	1.103 1.125 -0.022				
1.089 1.113 -0.024	1.258 1.239 0.019	1.093 1.119 -0.026			
1.252 1.234 0.018	1.084 1.110 -0.025	1.258 1.242 0.016	1.110 1.136 -0.026		
1.078 1.104 -0.025	1.246 1.230 0.016	1.082 1.110 -0.027	1.255 1.240 0.015	1.111 1.127 -0.016	
1.223 1.210 0.013	1.070 1.090 -0.020	1.240 1.225 0.015	1.117 1.133 -0.016	1.131 1.122 0.010	0.946 0.941 0.005
1.060 1.063 -0.003	1.083 1.074 0.009	0.913 0.926 -0.013	1.016 1.007 0.009	0.853 0.844 0.009	0.435 0.433 0.002
0.753 0.738 0.015	0.519 0.511 0.008	0.518 0.507 0.011	0.393 0.391 0.002		

PHOENIX/ANC
HELIOS/FORMOSA-P
Difference

FIGURE 6. PHOENIX/ANC vs. HELIOS/FORMOSA-P Assembly Power at 11 GWd/MTM

1.033 1.044 -0.011					
1.315 1.286 0.029	1.174 1.176 -0.002				
1.155 1.163 -0.008	1.318 1.301 0.017	1.156 1.169 -0.013			
1.315 1.295 0.020	1.149 1.159 -0.010	1.318 1.303 0.015	1.186 1.196 -0.010		
1.142 1.154 -0.012	1.312 1.291 0.021	1.150 1.163 -0.013	1.318 1.306 0.012	1.193 1.190 0.003	
1.295 1.278 0.017	1.149 1.166 -0.017	1.361 1.326 0.035	1.191 1.202 -0.011	1.266 1.234 0.032	1.178 1.170 0.008
1.227 1.232 -0.005	1.233 1.226 0.007	1.061 1.066 -0.005	1.224 1.208 0.016	1.151 1.148 0.003	0.728 0.738 -0.010
1.022 1.003 0.019	0.743 0.728 0.015	0.807 0.777 0.030	0.632 0.630 0.002		

PHOENIX/ANC
HELIOS/FORMOSA-P
Difference

FIGURE 7. PHOENIX/ANC vs. HELIOS/FORMOSA-P Peak Pin Power at 11 GWd/MTM

56.629 56.705 -0.076					
26.530 26.195 0.335	48.152 48.467 -0.315				
49.807 50.015 -0.208	26.846 26.576 0.270	49.762 50.099 -0.337			
26.762 26.483 0.279	50.068 50.353 -0.285	26.940 26.689 0.251	48.468 48.847 -0.379		
49.920 50.174 -0.254	26.736 26.453 0.283	50.021 50.317 -0.296	27.012 26.764 0.248	44.714 44.926 -0.212	
26.367 26.089 0.278	46.612 46.797 -0.185	26.754 26.429 0.325	46.303 46.430 -0.127	24.585 24.341 0.244	20.657 20.460 0.197
39.345 39.023 0.322	23.507 23.259 0.248	46.502 46.390 0.112	22.109 21.854 0.255	18.657 18.416 0.241	36.396 35.988 0.408
16.360 15.959 0.401	41.057 40.358 0.699	29.831 29.294 0.537	35.528 35.094 0.434		

PHOENIX/ANC
HELIOS/FORMOSA-P
Difference

Unit = GWd/MTM

FIGURE 8. PHOENIX/ANC vs. HELIOS/FORMOSA-P Assembly Burnup at 21.564 GWd/MTM

1.004 1.008 -0.004					
1.256 1.213 0.043	1.091 1.099 -0.008				
1.078 1.088 -0.010	1.260 1.220 0.040	1.078 1.091 -0.013			
1.255 1.217 0.038	1.071 1.085 -0.014	1.256 1.221 0.035	1.088 1.105 -0.016		
1.065 1.083 -0.018	1.247 1.216 0.031	1.065 1.086 -0.021	1.246 1.221 0.025	1.087 1.102 -0.015	
1.219 1.199 0.020	1.053 1.071 -0.018	1.241 1.217 0.024	1.089 1.109 -0.020	1.139 1.124 0.015	0.962 0.958 0.004
1.036 1.053 -0.017	1.079 1.074 0.005	0.921 0.941 -0.020	1.017 1.015 0.002	0.841 0.857 -0.016	0.460 0.479 -0.019
0.757 0.773 -0.016	0.550 0.563 -0.013	0.555 0.564 -0.009	0.423 0.443 -0.020		

PHOENIX/ANC
HELIOS/FORMOSA-P
Difference

FIGURE 9. PHOENIX/ANC vs. HELIOS/FORMOSA-P Assembly Power at 21.564 GWd/MTM

1.046 1.038 0.008					
1.302 1.252 0.050	1.150 1.136 0.014				
1.137 1.127 0.010	1.303 1.256 0.047	1.133 1.127 0.006			
1.298 1.252 0.046	1.130 1.122 0.008	1.299 1.257 0.042	1.144 1.147 -0.003		
1.125 1.120 0.005	1.291 1.251 0.040	1.127 1.125 0.002	1.295 1.261 0.034	1.155 1.152 0.003	
1.277 1.243 0.034	1.120 1.128 -0.008	1.321 1.272 0.049	1.157 1.160 -0.003	1.248 1.218 0.030	1.174 1.154 0.020
1.177 1.186 -0.008	1.212 1.193 0.019	1.042 1.054 -0.012	1.195 1.180 0.015	1.106 1.106 0.000	0.740 0.758 -0.018
1.014 1.001 0.013	0.761 0.760 0.001	0.821 0.814 0.006	0.664 0.671 -0.007		

PHOENIX/ANC
HELIOS/FORMOSA-P
Difference

FIGURE 10. PHOENIX/ANC vs. HELIOS/FORMOSA-P Peak Pin Power at 21.564 GWd/MTM

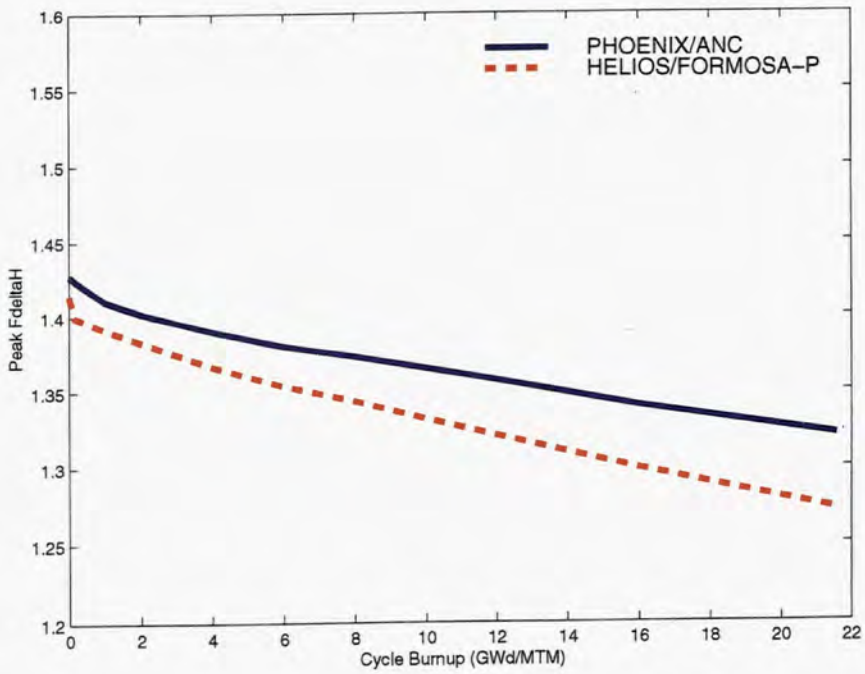

FIGURE 11. PHOENIX/ANC versus HELIOS/FORMOSA-P Peak $F_{\Delta H}$

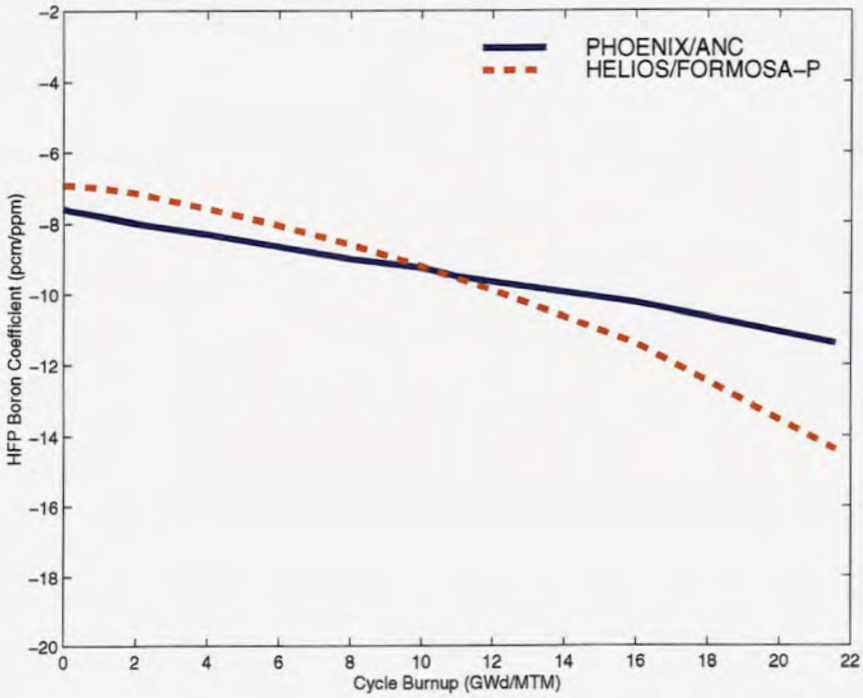

FIGURE 12. PHOENIX/ANC versus HELIOS/FORMOSA-P Boron Coefficients

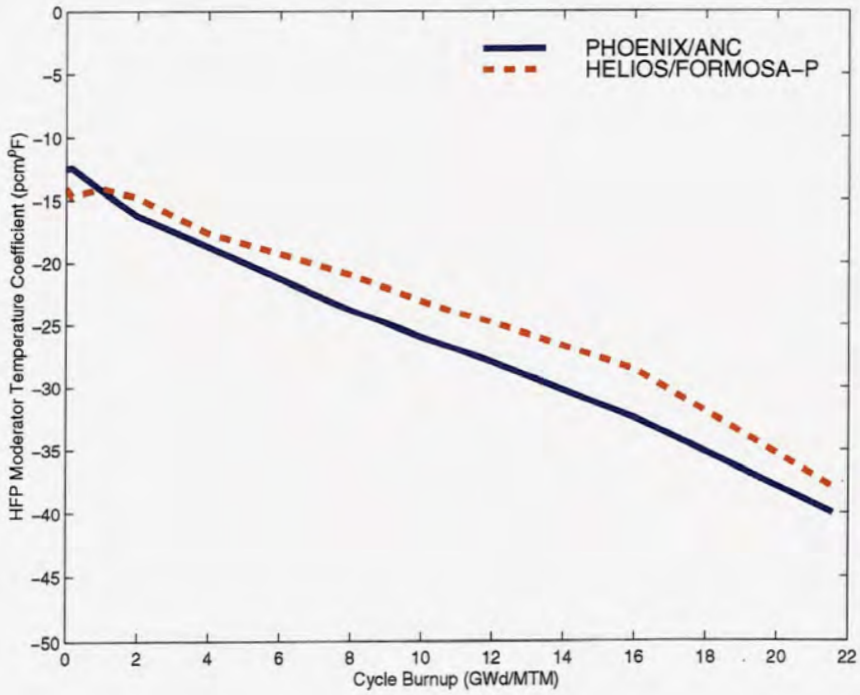

FIGURE 13. PHOENIX/ANC versus HELIOS/FORMOSA-P MTC

35.18 0.922 0.963					
0.000 1.173 1.289	24.34 1.077 1.141				
26.16 1.067 1.132	0.000 1.209 1.328	26.07 1.090 1.163			
0.000 1.209 1.326	26.53 1.078 1.146	0.000 1.238 1.360	24.34 1.145 1.239		
26.44 1.077 1.142	0.000 1.221 1.340	26.42 1.104 1.182	0.000 1.281 **1.414**	20.49 1.185 1.293	
0.000 1.212 1.336	23.27 1.080 1.171	0.000 1.240 1.410	21.87 1.180 1.271	0.000 1.217 1.372	0.000 1.036 1.328
16.03 1.056 1.262	0.000 1.089 1.296	26.41 0.896 1.067	0.000 1.064 1.337	0.000 0.946 1.355	26.64 0.426 0.800
0.000 0.715 1.026	29.39 0.446 0.679	18.45 0.433 0.715	26.72 0.343 0.595		

Assembly Burnup (GWd/MTM)
Assembly Power
Peak Pin Power
Twice-Burnt MOX
Once-Burnt MOX
Fresh MOX

bold denotes maximum value

FIGURE 14. Equilibrium Cycle, Full MOX Core Key Attributes at BOC Conditions

56.70 1.008 57.27					
26.19 1.213 27.97	48.47 1.099 49.87				
50.02 1.088 50.21	26.58 1.220 28.14	50.10 1.091 50.37			
26.48 1.217 28.06	50.35 1.085 50.42	26.69 1.221 28.29	48.85 1.105 50.06		
50.17 1.083 50.19	26.45 1.216 28.10	50.32 1.086 50.54	26.76 1.221 28.34	44.93 1.102 48.94	
26.09 1.199 27.83	46.80 1.071 49.16	26.43 1.217 29.76	46.43 1.109 50.72	24.34 1.124 27.19	20.46 0.958 25.62
39.02 1.053 41.49	23.26 1.074 26.68	46.39 0.941 51.41	21.85 1.015 26.87	18.42 0.857 24.69	35.99 0.479 44.53
15.96 0.773 22.98	40.36 0.563 45.71	29.30 0.564 31.29	35.10 0.443 42.16		

Assembly Burnup (GWd/MTM)
Assembly Power
Peak Pin Burnup (GWd/MTM)
Thrice-Burnt MOX
Twice-Burnt MOX
Once-Burnt MOX

bold denotes maximum value

FIGURE 15. Equilibrium Cycle, Full MOX Core Key Attributes at EOC Conditions

5. Initial Mixed LEU-MOX Core

Several scenarios (Figure 16) were examined in regard to mixed LEU-MOX cores starting with the equilibrium cycle, full MOX core. All scenarios have in common that the first cycle that LEU feed assemblies are loaded into the core, all MOX feed assemblies are unavailable and replaced by LEU feed assemblies. This will be referred to as the Initial Mixed LEU-MOX Core. In subsequent cycles, different scenarios are assumed depending upon the availability of MOX feed assemblies, as will be described in Section 6. For all scenarios, the LEU lattice designs used are the standard Westinghouse LEU lattice designs with uniform pin-wise enrichment distribution. The MOX lattice designs used in this study are also assumed to have uniform pin-wise enrichment distribution. As noted earlier, the LEU assemblies utilize IFBAs while MOX assemblies utilize WABAs as burnable absorbers.

For the initial mixed LEU-MOX core, the following design approach was employed. First, the non-dominant MOX feed batch, *i.e.* smaller size feed batch, is replaced by an LEU feed batch to find the "equivalent" LEU feed batch whose BP loading and ^{235}U enrichment produce the same cycle energy production and maximum soluble boron concentration for the first cycle loaded, utilizing the minimum non-dominant batch feed enrichment possible. In completing this assessment of the lattice attributes of the non-dominant LEU feed batch, the core LP is fixed and dominant MOX feed batch retained, with the only constraints imposed being those noted above, *i.e.* cycle energy requirement and maximum soluble boron concentration. This assessment is completed utilizing FORMOSA-P without automatic optimization capability activated. Using this approach, the non-dominant feed batch enrichment is determined to be 4.0 w/o ^{235}U.

Fixing the non-dominant LEU feed batch at the equivalent feed batch attributes, the dominant LEU feed batch is determined such that the cycle energy requirement (21,564 MWd/MTM) and all constraints [maximum soluble boron concentration (1,829 ppm), radial pin-wise power peaking (1.528), maximum pin-wise discharge burnup (60 GWd/MTHM), maximum assembly discharge burnup (57 GWd/MTM), and maximum region discharge burnup (45 GWd/MTM)] are satisfied and the dominant LEU feed batch enrichment is minimized. This is accomplished utilizing FORMOSA-P with the automatic optimization capability activated. During optimizations, fresh assemblies locations are

fixed to their original locations (as in the equilibrium cycle, full MOX core) while burnt assemblies are allowed to shuffle. BP loadings for both minor and major feed batches are determined via FORMOSA-P optimizations. The number of BPs available for selections are 0, 16, 48, 64, 80, 104, and 128 IFBA rods per assembly. The major feed batch enrichment determined by FORMOSA-P is 3.5 w/o ^{235}U. The initial mixed core loading pattern is shown in Figure 17, and some key core attributes at BOC and EOC conditions are shown in Figure 18 and Figure 19, respectively. The maximum pin power is found to be 1.518, higher than the maximum value for the full MOX core, but within the limit imposed of 1.528. The maximum pin power occurs in a once-burnt MOX assembly in a pin located on the edge of the assembly whose surface is adjacent to a fresh LEU assembly. Apparently, thermal neutron diffusion from the LEU to MOX assembly, caused by the much softer energy spectrum in the LEU assembly, is causing the power peaking in the adjacent MOX assembly. All the other constraints imposed are satisfied.

The resulting LP for the initial mixed LEU-MOX core is the starting point for the optimization of subsequent cycles as now explained.

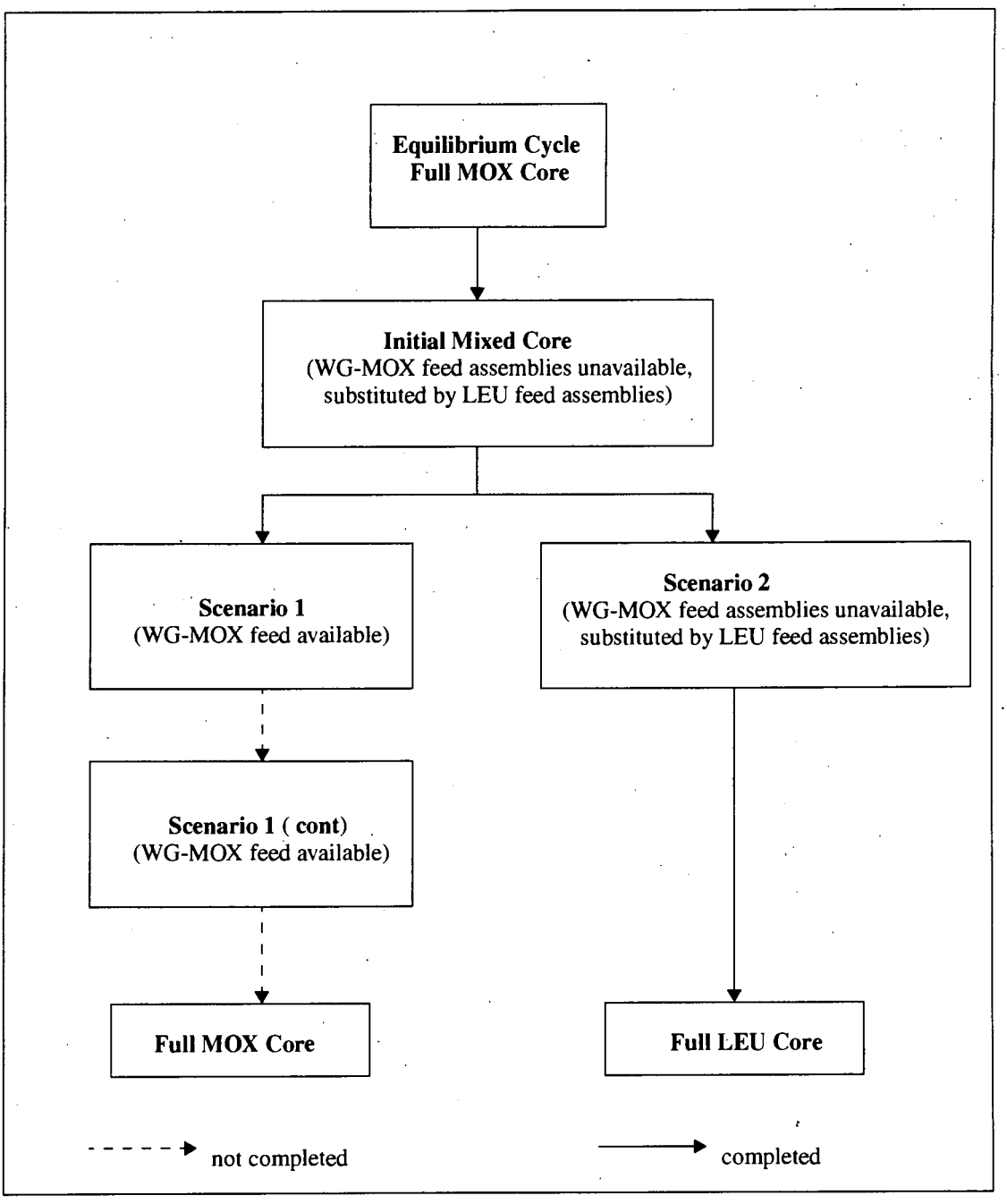

FIGURE 16. Mixed Core Scenarios

M-4.0 **W-0**					
L-3.5 **I-128**	**M-4.0** **W-0**				
M-4.0 **W-0**	**L-3.5** **I-0**	**M-4.0** **W-0**			
L-3.5 **I-80**	**M-4.0** **W-0**	**L-3.5** **I-80**	**M-4.0** **W-0**		
M-4.0 **W-0**	**L-3.5** **I-16**	**M-4.0** **W-0**	**L-3.5** **I-64**	**M-4.0** **W-0**	
L-3.5 **I-128**	**M-4.0** **W-0**	**L-4.0** **I-80**	**M-4.5** **W-0**	**L-3.5** **I-16**	**L-3.5** **I-0**
M-4.5 **W-0**	**L-3.5** **I-16**	**M-4.5** **W-0**	**L-4.0** **I-0**	**L-3.5** **I-0**	**M-4.0** **W-0**
L-4.0 **I-0**	**M-4.0** **W-0**	**M-4.0** **W-0**	**M-4.0** **W-0**		

Twice-Burnt
Once-Burnt
Fresh

Fuel type - enrichment
BA type - # BA

M=MOX, L=LEU
W=WABA, I=IFBA

FIGURE 17. Initial Mixed Core Loading Pattern

29.39 0.890 1.046					
0.000 0.938 1.074	26.44 1.135 1.503				
26.16 1.196 1.453	0.000 1.279 1.455	26.07 1.253 1.515			
0.000 1.158 1.275	26.64 1.246 1.467	0.000 1.153 1.273	24.34 1.235 1.484		
24.34 1.253 1.500	0.000 1.271 1.432	23.27 1.256 1.489	0.000 1.176 1.313	20.49 1.250 1.515	
0.000 1.044 1.173	18.45 1.243 1.512	0.000 1.201 1.352	21.87 1.248 **1.518**	0.000 1.127 1.297	0.000 0.888 1.176
16.03 1.120 1.498	0.000 1.000 1.213	26.41 0.960 1.414	0.000 0.967 1.243	0.000 0.722 1.069	26.72 0.388 1.019
0.000 0.634 0.912	26.42 0.516 0.974	26.53 0.415 0.690	35.18 0.296 0.616		

Assembly Burnup (GWd/MTM)
Assembly Power
Peak Pin Power
Twice-Burnt MOX
Once-Burnt MOX
Fresh LEU

bold denotes maximum value

FIGURE 18. Initial Mixed Core Key Attributes at BOC Conditions

51.45 **1.041** **56.75**					
24.52 1.160 26.86	50.52 1.075 58.67				
50.58 1.074 58.26	25.98 1.139 28.55	50.91 1.075 58.62			
25.76 1.149 28.17	51.42 1.073 59.11	26.01 1.159 28.50	49.83 1.111 57.07		
49.73 1.104 57.80	26.52 1.163 29.15	48.85 1.114 57.78	26.30 1.184 28.99	45.83 1.136 53.44	
25.54 1.182 28.05	44.13 1.137 55.94	26.95 1.225 29.77	47.46 1.158 60.00	24.17 1.155 27.25	19.61 1.001 24.90
40.07 1.117 50.92	22.31 1.066 26.34	46.94 0.976 58.20	20.97 1.033 25.47	16.37 0.865 23.12	35.86 0.515 50.60
14.87 0.785 20.12	38.30 0.622 50.80	36.25 0.525 43.42	42.25 0.402 56.10		

Assembly Burnup (GWd/MTM)
Assembly Power
Peak Pin Burnup (GWd/MTM)
Thrice-Burnt MOX
Twice-Burnt MOX
Once-Burnt LEU

bold denotes maximum value

FIGURE 19. Initial Mixed Core Key Attibutes at EOC Conditions

6. Subsequent Mixed LEU-MOX Cores

Starting with the initial mixed core defined in Section 5, two scenarios (see Figure 16) are introduced in regard to availability of MOX feed assemblies in the subsequent cycle: (1) assume that MOX feed batches are available and (2) assume that MOX feed batches continue to be unavailable. LEU lattice designs are limited to standard Westinghouse designs which employ uniform pin-wise enrichment distributions. MOX lattice designs are limited to MOX designs used in the Westinghouse equilibrium cycle full MOX core, which also employ uniform pin-wise enrichment distributions. This was done to determine if acceptable LPs could be determined without the need to develop new and more complex lattice designs.

6.1 Scenario 1: MOX Feed Batches Available for Subsequent Cycle

MOX feed batch attributes are determined using FORMOSA-P optimizations in manners similar to determining the feed batch attributes for the initial mixed core. The objective of FORMOSA-P optimizations is to minimize the major feed batch enrichment. As before, during optimizations, fresh assembly locations are fixed to their original locations (as in the equilibrium cycle, full MOX core) while burnt assemblies are allowed to shuffle. BP loadings for both minor and major feed batches are also determined via FORMOSA-P optimizations using the WABA designs.

Currently, we have not found a loading pattern which satisfies the maximum pin power limit, with numerous violations occurring. As mentioned before, the MOX lattice designs employed are limited to the MOX designs used in the Westinghouse equilibrium cycle, full MOX core. The designs employ uniform pin-wise enrichment distribution. Figure 21 and Figure 22 show that when a fresh MOX assembly is adjacent to a once-burnt LEU assembly, pin powers for the pins in the outer rows of the MOX assembly are very high relative to the assembly average power. This suggests that pin-wise enrichment zoning might be necessary to control the peak pin power. Indeed, this was the approach taken by Westinghouse during the transition cycles from a full LEU core to full MOX core. Note that the discharge burnup (Figure 23) and boron concentration limits for this scenario are already satisfied. The feed enrichments determined (Figure 20) should be acceptable with regard to criticality limitations.Reemploying FORMOSA-P and removing the restriction of freezing the fresh assemblies locations at their original locations did not result in any reduction in the peak pin power.

M-4.0 W-0					
M-4.4 W-24	L-3.5 I-0				
L-3.5 I-128	M-4.4 W-12	L-3.5 I-0			
M-4.4 W-0	L-3.5 I-16	M-4.4 W-12	L-3.5 I-80		
L-3.5 I-128	M-4.4 W-12	L-3.5 I-80	M-4.4 W-24	L-3.5 I-0	
M-4.4 W-12	L-3.5 I-16	M-4.8 W-12	L-3.5 I-0	M-4.4 W-12	M-4.4 W-0
L-4.0 I-0	M-4.4 W-0	L-4.0 I-0	M-4.8 W-0	M-4.4 W-0	L-3.5 I-64
M-4.8 W-0	L-4.0 I-80	L-3.5 I-16	M-4.0 W-0		

Twice-Burnt
Once-Burnt
Fresh

Fuel type - enrichment
BA type - # BA

M=MOX, L=LEU
W=WABA, I=IFBA

FIGURE 20. Scenario 1 Loading Pattern

36.36 0.823 0.863					
0.000 1.130 **1.568**	19.73 0.862 0.952				
24.46 0.887 0.990	0.000 1.314 **1.679**	25.91 0.855 0.920			
0.000 1.52 **1.728**	26.43 0.900 0.991	0.000 1.298 **1.630**	25.69 0.834 0.909		
25.48 0.948 1.028	0.000 1.385 **1.726**	25.92 0.876 0.968	0.000 1.220 **1.736**	25.91 0.925 1.062	
0.000 1.427 **1.745**	22.34 0.953 1.059	0.000 1.399 **1.756**	16.52 1.014 1.174	0.000 1.481 **1.746**	0.000 1.354 **1.730**
15.00 0.991 1.207	0.000 1.285 **1.715**	21.05 0.819 1.034	0.000 1.265 **1.731**	0.000 1.110 **1.565**	26.23 0.405 0.758
0.000 0.766 1.263	26.89 0.422 0.670	24.20 0.317 0.537	35.99 0.311 0.587		

Assembly Burnup (GWd/MTM)
Assembly Power
Peak Pin Power
Twice-Burnt MOX
Once-Burnt LEU
Fresh MOX

bold denotes violations

FIGURE 21. Scenario 1 Core Key Attributes at BOC Conditions

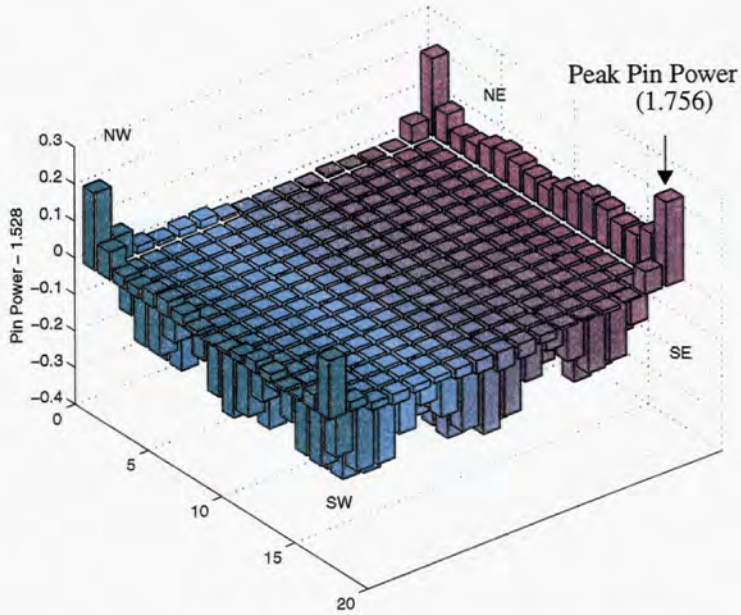

FIGURE 22. Pin Power Distribution in Scenario 1

(Assembly location is shown by bold edges in Figure 21)

57.67 1.020 **58.31**					
27.60 1.293 37.95	41.69 1.034 46.82				
45.95 0.994 50.36	29.21 1.304 38.90	46.77 0.978 51.27			
30.55 1.305 39.82	47.44 0.969 51.94	28.63 1.296 38.31	46.06 0.982 50.46		
46.91 0.977 51.39	29.14 1.293 38.86	46.65 0.982 51.11	27.08 1.281 37.27	46.17 0.966 50.94	
29.32 1.295 38.88	43.83 0.993 49.68	29.12 1.317 40.27	38.42 1.022 44.46	27.01 1.200 37.85	23.27 1.028 28.55
37.06 1.022 42.43	26.26 1.186 38.63	39.82 0.912 44.11	24.05 1.087 38.76	19.79 0.895 27.02	34.63 0.433 41.83
17.21 0.845 31.44	37.72 0.582 44.51	32.85 0.491 38.00	43.30 0.395 54.41		

Assembly Burnup (GWd/MTM)
Assembly Power
Peak Pin Burnup (GWd/MTM)
Thrice-Burnt MOX
Twice-Burnt LEU
Once-Burnt MOX

FIGURE 23. Scenario 1 Core Key Attributes at EOC Conditions

6.2 Scenario 2: MOX Feed Batches Continue to be Unavailable for Subsequent Cycle

For this scenario, MOX feed assemblies are assumed to continue to be unavailable and are replaced by LEU feed assemblies. Figure 24 presents the loading pattern determined by FORMOSA-P employing the objective of minimizing the major feed batch enrichment. As before, during optimizations fresh assemblies locations are fixed to their original locations (as in the equilibrium cycle, full MOX core) while burnt assemblies are allowed to shuffle. BP loadings for both minor and major feed batches are determined via the FORMOSA-P optimization using the IFBA design. The LEU enrichments for the major and minor feed batches are within the critical material limits for fuel fabrication and spent fuel pool storage (5.0 w/o ^{235}U). BOC and EOC conditions are shown in Figure 25 and Figure 26, respectively. The maximum $F_{\Delta H}$ (1.462) is well within the limit imposed of 1.528. The maximum pin discharge burnup (59.52 GWd/MTM) is also within the limit imposed.

M-4.0 W-0					
L-4.1 I-128	L-3.5 I-0				
L-3.5 I-0	L-4.1 I-80	L-3.5 I-128			
L-4.1 I-80	L-3.5 I-16	L-4.1 I-80	L-3.5 I-128		
L-3.5 I-80	L-4.1 I-80	L-3.5 I-16	L-4.1 I-104	L-3.5 I-0	
L-4.1 I-80	L-4.0 I-0	L-4.5 I-104	L-3.5 I-0	L-4.1 I-128	L-4.1 I-0
L-4.0 I-0	L-4.1 I-80	L-4.0 I-80	L-4.5 I-0	L-4.1 I-0	L-3.5 I-16
L-4.5 I-0	L-3.5 I-80	L-3.5 I-64	M-4.0 W-0		

Twice-Burnt
Once-Burnt
Fresh

Fuel type - enrichment
BA type - # BA

M=MOX, L=LEU
W=WABA, I=IFBA

FIGURE 24. Scenario 2 Loading Pattern

36.36 0.830 1.031					
0.000 0.983 1.065	25.91 0.874 0.965				
25.91 0.930 1.004	0.000 1.186 1.268	25.48 1.005 1.054			
0.000 1.263 1.343	24.20 1.032 1.084	0.000 1.283 1.357	24.46 1.045 1.077		
25.69 1.086 1.138	0.000 1.348 1.433	22.34 1.110 1.184	0.000 1.255 1.316	19.73 1.054 1.132	
0.000 1.371 1.443	21.05 1.206 1.262	0.000 1.348 1.414	16.52 1.132 1.258	0.000 1.166 1.253	0.000 1.064 1.338
15.00 1.129 1.225	0.000 1.116 1.309	26.89 0.887 1.142	0.000 1.198 **1.462**	0.000 0.920 1.291	26.43 0.377 0.809
0.000 0.766 1.110	25.92 0.456 0.797	26.23 0.372 0.627	35.99 0.347 0.800		

Assembly Burnup (GWd/MTM)
Assembly Power
Peak Pin Power
Twice-Burnt MOX
Once-Burnt LEU
Fresh LEU

bold denotes maximum value

FIGURE 25. Scenario 2 Core Key Attributes at BOC Conditions

57.70 1.006 **59.52**					
26.59 1.205 27.69	46.77 0.973 49.07				
47.00 0.970 49.16	27.71 1.247 28.08	47.08 0.972 49.21			
28.08 1.245 28.45	45.97 0.976 48.69	28.34 1.249 28.71	46.60 0.989 48.53		
47.65 0.980 49.70	28.76 1.260 29.11	45.15 1.013 48.47	28.64 1.278 29.06	42.60 1.040 46.51	
28.6 1.272 28.99	44.99 1.070 48.95	29.14 1.310 30.79	39.60 1.048 45.31	27.08 1.254 28.86	22.86 1.080 28.29
37.45 1.060 43.43	24.11 1.166 27.41	44.95 0.880 48.30	23.35 1.094 28.47	19.11 0.930 26.43	34.93 0.458 40.99
16.12 0.855 23.17	35.97 0.560 41.18	34.44 0.469 39.09	43.29 0.398 51.89		

Assembly Burnup (GWd/MTM)
Assembly Power
Peak Pin Burnup (GWd/MTM)
Thrice-Burnt MOX
Twice-Burnt LEU
Once-Burnt LEU

bold denotes maximum value

FIGURE 26. Scenario 2 Core Key Attributes at EOC Conditions

6.3 Transition Back to Full LEU Core

Continuing Scenario 2, which assumes the unavailability of MOX feed assemblies, a transition back to a full LEU core occurs. Figure 27 presents the loading pattern determined by FORMOSA-P for this condition, employing the objective of minimizing the major feed batch enrichment. As before, during optimization, fresh assemblies locations are fixed to their original locations (as in the equilibrium cycle, full MOX core) while burnt assemblies are allowed to shuffle. BP loadings for both minor and major feed batches are determined via FORMOSA-P optimization utilizing the IFBA design. The LEU enrichments for the major and minor feed batches are well within the criticality limits. From Figure 28 and Figure 29 it can be seen that pin power and discharge burnup limits are all satisfied for the optimum LP identified by FORMOSA-P.

L-3.5 I-16					
L-3.9 I-128	L-4.1 I-80				
L-4.1 I-80	L-3.9 I-80	L-4.1 I-80			
L-3.9 I-80	L-4.1 I-128	L-3.9 I-80	L-4.1 I-128		
L-4.1 I-80	L-3.9 I-80	L-4.1 I-80	L-3.9 I-104	L-4.1 I-0	
L-3.9 I-80	L-4.5 I-0	L-4.4 I-104	L-4.1 I-0	L-3.9 I-128	L-3.9 I-0
L-4.5 I-0	L-3.9 I-80	L-4.5 I-104	L-4.4 I-0	L-3.9 I-0	L-4.1 I-104
L-4.4 I-0	L-4.1 I-80	L-3.5 I-64	L-4.1 I-80		

Twice-Burnt
Once-Burnt
Fresh

Fuel type - enrichment
BA type - # BA

M=MOX, L=LEU
W=WABA, I=IFBA

FIGURE 27. Full LEU Core Loading Pattern

35.03 0.638 0.653					
0.000 0.909 0.994	28.24 0.872 0.957				
28.24 0.948 1.019	0.000 1.147 1.240	27.99 1.037 1.095			
0.000 1.234 1.322	27.03 1.086 1.169	0.000 1.274 1.358	26.51 1.114 1.152		
28.54 1.125 1.178	0.000 1.329 1.417	24.16 1.180 1.256	0.000 1.250 1.302	22.88 1.111 1.172	
0.000 1.344 1.422	23.39 1.246 1.306	0.000 1.346 1.414	19.19 1.199 1.296	0.000 1.128 1.228	0.000 1.015 1.281
16.29 1.181 1.264	0.000 1.086 1.287	29.07 0.889 1.088	0.000 1.182 **1.446**	0.000 0.881 1.248	28.54 0.381 0.799
0.000 0.771 1.116	27.62 0.472 0.815	34.58 0.317 0.532	28.66 0.322 0.626		

Assembly Burnup (GWd/MTM)
Assembly Power
Peak Pin Power
Twice-Burnt LEU
Once-Burnt LEU
Fresh LEU

FIGURE 28. Full LEU Core Key Attributes at BOC Conditions

52.84 0.897 **53.05**					
25.62 1.234 26.07	49.55 1.003 50.91				
50.00 1.000 51.12	27.13 1.222 27.49	50.30 0.997 51.45			
27.55 1.217 27.87	49.79 1.007 51.38	28.04 1.223 28.39	49.79 1.023 50.86		
51.21 1.001 51.58	28.32 1.232 28.80	48.17 1.049 51.00	28.33 1.252 28.65	46.68 1.072 51.69	
28.09 1.246 28.67	48.03 1.093 52.96	28.95 1.295 30.01	43.36 1.087 50.16	26.35 1.231 27.48	22.03 1.060 27.40
39.64 1.096 47.66	23.58 1.143 26.49	47.25 0.892 52.75	23.06 1.094 27.69	18.43 0.913 25.66	37.21 0.476 46.26
16.10 0.852 22.88	37.99 0.579 44.63	41.72 0.421 48.83	35.63 0.402 41.59		

Assembly Burnup (GWd/MTM)
Assembly Power
Peak Pin Burnup (GWd/MTM)
Thrice-Burnt LEU
Twice-Burnt LEU
Once-Burnt LEU

bold denotes maximum value

FIGURE 29. Full LEU Core Key Attributes at EOC Conditions

6.4 Summary of Key Core Attributes

Table 2 summarizes the feed enrichments used in the various cores being studied. The feed enrichments for all cores examined satisfy the criticality limit. Soluble boron concentrations, $F_{\Delta H}$, HFP boron worth, and HFP MTC as a function of cycle burnup for the various cores examined are presented in Figure 30 through Figure 33. The indicated behaviors are as to be expected based upon the size and burnups of MOX and LEU batches within the core.

TABLE 2: Feed Enrichment for Various Cores

Core	Feed Batch Enrichment	
	20 Assemblies	72 Assemblies
Equilibrium Cycle, Full MOX	4.5 w/o WGPu	4.0 w/o WGPu
Initial Mixed Core	4.0 w/o ^{235}U	3.5 w/o ^{235}U
Scenario 1	4.8 w/o WGPu	4.4 w/oWGPu
Scenario 2	4.5 w/o ^{235}U	4.1 w/o ^{235}U
Full LEU	4.4 w/o ^{235}U	3.9 w/o ^{235}U

TABLE 3: Core Performance for Various Cores

Core	Maximum Soluble Boron (ppm)	Maximum Pin Power	Maximum Pin Discharge Burnup (GWD/ MTM)
Equilibrium Cycle, Full MOX	1385	1.414	57.27
Initial Mixed Core	941	1.518	56.75
Scenario 1	1341	**1.756**	58.31
Scenario 2	750	1.460	59.52
Full LEU	750	1.446	53.05
Limit	1829	1.528	60.00

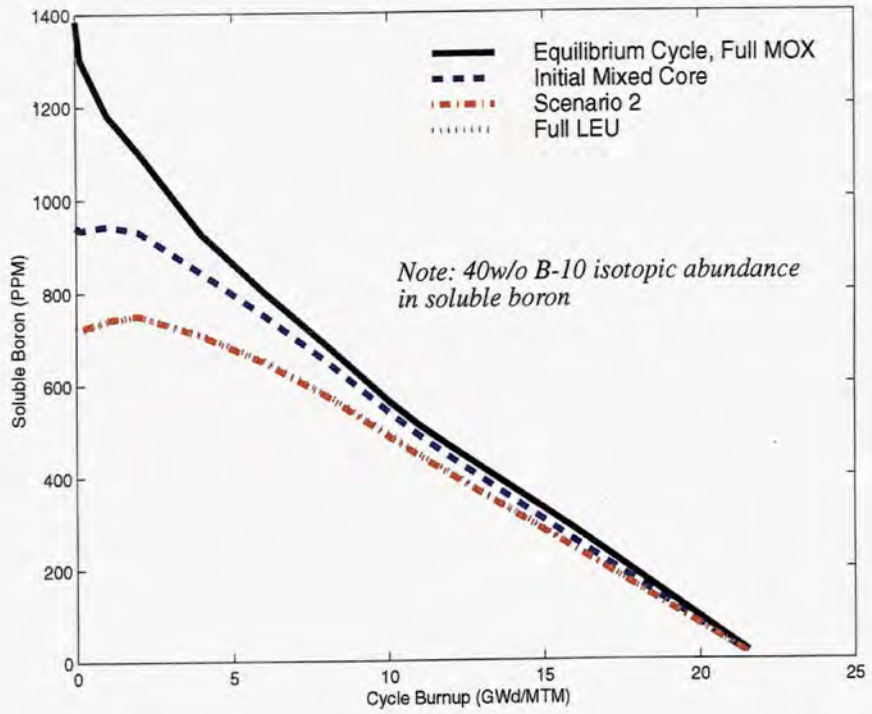

FIGURE 30. Soluble Boron Concentration vs. Cycle Burnup

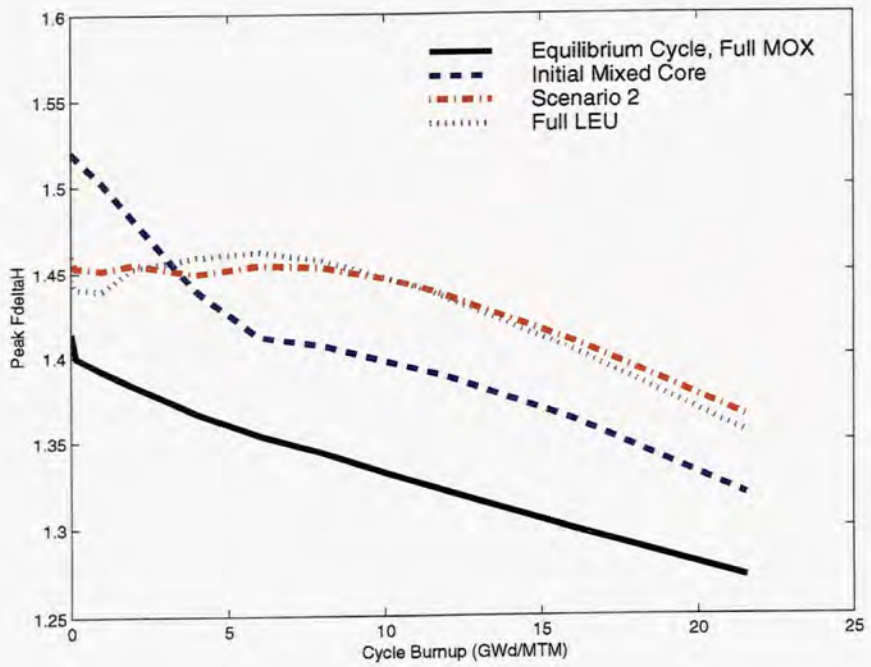

FIGURE 31. Peak $F_{\Delta H}$ vs. Cycle Burnup

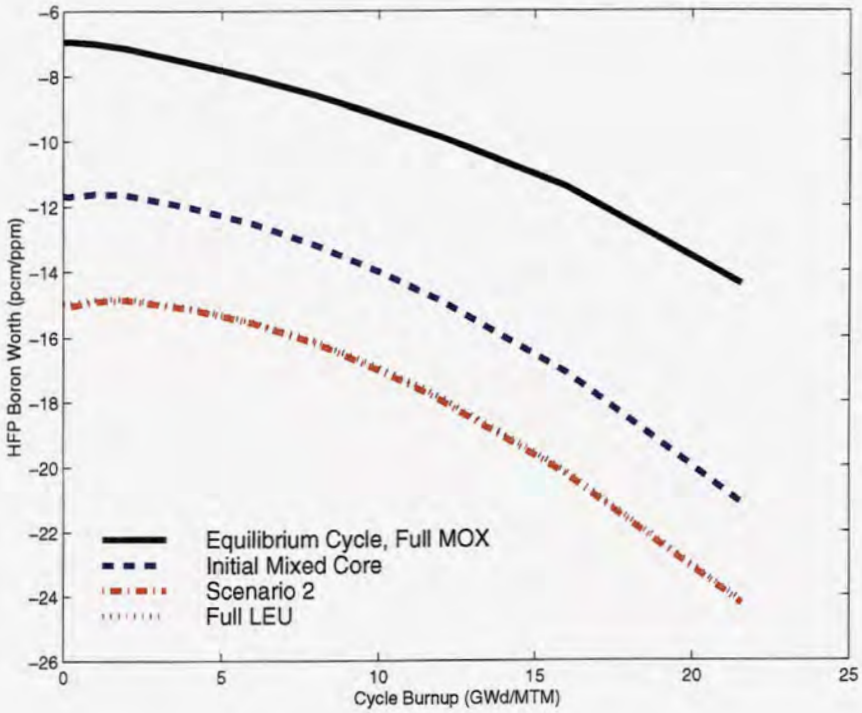

FIGURE 32. HFP Boron Worth vs. Cycle Burnup

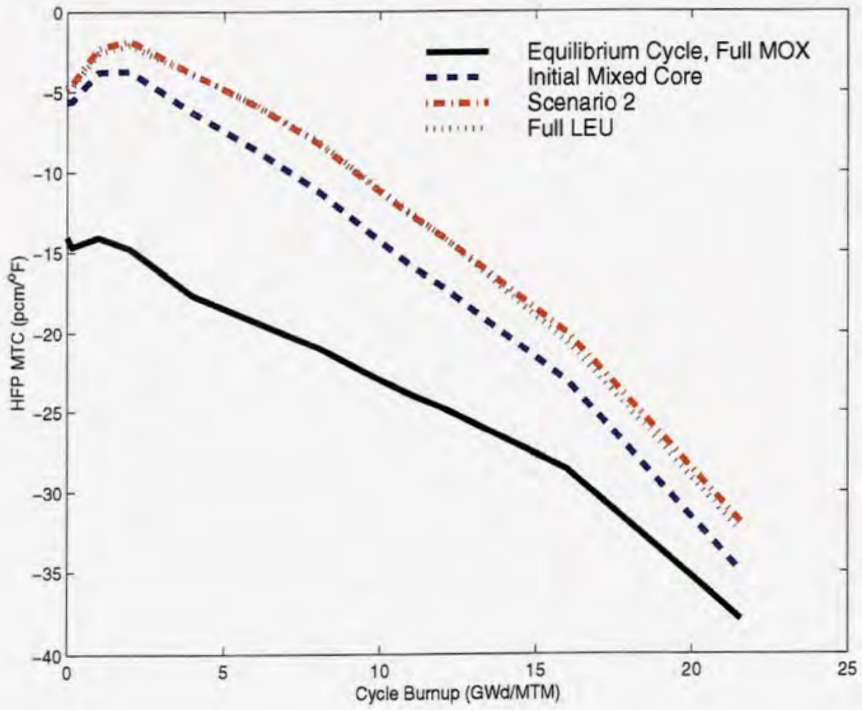

FIGURE 33. HFP MTC vs. Cycle Burnup

7. Conclusions

For the initial mixed LEU-MOX core, starting with the Westinghouse equilibrium cycle, full MOX core, an acceptable LP was determined in regard to satisfying all constraints. For the subsequent cycle, the following two disruption scenarios were examined: (1) complete availability of MOX feed assemblies and (2) complete unavailability of MOX feed assemblies.

The first scenario leads to a full MOX core. No LP could be determined which satisfied the maximum pin power constraint. Maximum pin power violations occur in almost all fresh MOX assemblies adjacent to burnt LEU assemblies. Modification of the lattice design, which was restricted in this study to uniform pin enrichments within an assembly as utilized in the equilibrium cycle, full MOX core, should be pursued to control the peak pin power by minimizing the adverse LEU-MOX assemblies interfacial effects.

The second scenario leads to a full LEU core. Transition cycles from an equilibrium cycle, full MOX core to a full LEU core have been developed. LPs found by FORMOSA-P for those transition cycles satisfy all constraints imposed.

8. Acknowledgment

The authors would like to thank Dr. Trent Primm of Oak Ridge National Laboratory, Dr. Marvin Adams and Mr. Gustavo Alonso-Vargas of Texas A&M University, and Mr. Rick Ankney of Westinghouse Electric Company for their cooperation during the course of this study.

9. References

[1] "Plutonium Disposition Study: Implementation of Weapons Grade MOX Fuel in Existing Pressurized Water Reactors" Contract No. DE-AC03-93SF-19683, Westinghouse Electric Corporation (1996).

[2] "FMS: The Scanpower Fuel Management System, HELIOS Documentation," Scanpower A/S (1995).

[3] "FORMOSA-P V3.6.0 User's Manual: Fuel Management Optimization Software for PWRs," Electric Power Research Center, North Carolina State University (1998).

[4] "FORCIP-P Version 2.1 Code Manual: FORMOSA-P cross Section Interface Program," Electric Power Research Center, North Carolina State University (1998).

INTERNAL DISTRIBUTION

1. M. D. DeHart
2. R. J. Ellis
3. J. C. Gehin
4. S. R. Greene
5. S. A. Hodge
6. D. T. Ingersoll
7. M. A. Kuliasha
8. S. B. Ludwig
9. G. E. Michaels
10. D. L. Moses
11. B. D. Murphy
12. D. G. O'Connor
13–17. R. T. Primm, III
18. C. C. Southmayd
19–23. D. J. Spellman
24. R. M. Westfall
25. K. A. Williams
26. B. A. Worley
27. Central Research Library
28. FMDP Library
29–30. ORNL Laboratory Records (OSTI)
31. ORNL Laboratory Records–RC

EXTERNAL DISTRIBUTION

32. M. L. Adams, Department of Nuclear Engineering, Texas A&M University, Zachry 129, College Station, TX 77843
33. Dave Alberstein, LANL, P.O. Box 1663, MS-K575, Los Alamos, NM 87545
34. G. Alonszo, Department of Nuclear Engineering, P.O. Box 7909, North Carolina State University, Raleigh, NC 27695-7909
35. Richard D. Ankney, Westinghouse Electric Company, P.O. Box 355, Pittsburgh, PA 15230-0355
36. Imelda Ariani, Department of Nuclear Engineering, P.O. Box 7909, North Carolina State University, Raleigh, NC 27695-7909
37. Tim Barr, DOE, Chicago Operations Office, 9700 S. Cass Avenue, Chicago, IL 60439
38. H. R. Canter, Office of Fissile Materials Disposition, U.S. Department of Energy, MD-1/2, 1000 Independence Avenue SW, Washington DC 20585
39. G. S. Chang, INEEL, P.O. Box 1625, MS-3885, Idaho Falls, ID 83415-3885
40. A. I. Cygelman, Department of Energy, 1000 Independence Avenue SW, Forrestal Building 3F043, Washington, DC 20585
41. L. Groves, Sandia National Laboratories, P.O. Box 969, Livermore, CA 94551
42. D. Harrison, Department of Energy, 101 Convention Center Drive, Suite P200, Las Vegas, NV 89109
43. G. Holman, Lawrence Livermore National Laboratory, P.O. Box 808, Livermore, CA 94551
44. C. Jaeger, Sandia National Laboratories, P.O. Box 5800, Albuquerque, NM 78185-0759
45. Frank Motley, LANL, P.O. Box 1663, MS-K575, Los Alamos, NM 87545

46–50. Office of the ORNL Site Manager, Department of Energy, Oak Ridge National Laboratory, P.O. Box 2008, Oak Ridge, TN 37831

51. D. Peko, Department of Energy, 1000 Independence Avenue SW, Forrestal Building 3F042, Washington, DC 20585
52. P. T. Rhoads, Office of Fissile Materials Disposition, U.S. Department of Energy, MD-4, 1000 Independence Avenue SW, Washington, DC 20585
53. G. P. Rudy, Department of Energy, 1000 Independence Avenue SW, Forrestal Building 7B192, Washington, DC 20585
54. J. M. Ryskamp, INEEL, P.O. Box 1625, MS-3885, Idaho Falls, ID 83415-3885
55. Robert Selby, DOE, Chicago Operations Office, 9700 S. Cass Avenue, Chicago, IL 60439
56. J. Thompson, Office of Fissile Materials Disposition, U.S. Department of Energy, MD-4, 1000 Independence Avenue SW, Forrestal Building 3F043, Washington, DC 20585
57. Dr. Paul Turinsky, Department of Nuclear Engineering, North Carolina State University, Raleigh, NC 27695-7909